

Polarization-momentum hyperentangled states: Realization and characterization

M. Barbieri, C. Cinelli, P. Mataloni, and F. De Martini

Dipartimento di Fisica dell' Universita' "La Sapienza" and Consorzio Nazionale Interuniversitario per le Scienze Fisiche della Materia, Roma, 00185 Italy

(Received 27 July 2005; published 17 November 2005)

We present an experimental method to engineer polarization-momentum hyperentangled two-photon states, using linear optics and a single type-I nonlinear crystal. These states have been completely characterized and their nonlocal behavior has been verified by an “all versus nothing” test of local realism, which represents a generalization of the Greenberger-Horne-Zeilinger (GHZ) to the case of two entangled particles and two observers. The manipulation of these states may represent a useful control in quantum state engineering and Bell state measurements and, more in general, in quantum information applications.

DOI: [10.1103/PhysRevA.72.052110](https://doi.org/10.1103/PhysRevA.72.052110)

PACS number(s): 03.65.Ud, 03.67.–a, 03.67.Mn, 03.67.Hk

I. INTRODUCTION

Entanglement represents the key resource for quantum information (QI). It combines three basic structural elements of quantum theory: the superposition principle, the quantum nonseparability property, and the exponential scaling of the state space with the number of partitions. This unique resource, associated with peculiar nonclassical correlations among separated quantum systems, can be used to perform computational and cryptographic tasks that are impossible for classical systems [1–3]. Quantum optics has represented an excellent experimental test benchmark for various novel concepts introduced within QI theory, such as quantum dense coding [4], teleportation [5,6], and entanglement swapping [7]. By the spontaneous parametric down conversion (SPDC) process pairs of correlated photons are generated by shining a nonlinear (NL) optical crystal by a pump laser beam [8]. Entangled pure or (controllable) mixed states are generated in this way and photon qubits can be encoded in polarization or energy or momentum directions. Concerning polarization entanglement, the bipartite 2×2 Hilbert space is spanned by the four Bell states

$$|\Psi^\pm\rangle = \frac{1}{\sqrt{2}}(|H\rangle|V\rangle \pm |V\rangle|H\rangle), \quad |\Phi^\pm\rangle = \frac{1}{\sqrt{2}}(|H\rangle|H\rangle \pm |V\rangle|V\rangle) \quad (1)$$

expressed in the horizontal (H) and vertical (V) polarization basis. On the practical side, single photons or photon pairs are ideal carriers of information for quantum communication since they can be distributed over long distances in free space and in low-loss optical fibers. Photon states can be easily and accurately manipulated using linear and nonlinear optical devices and can be efficiently measured by means of single-photon detectors.

An intrinsic limit of SPDC is that no more than one photon pair is created time by time within each microscopic annihilation-creation process. This can represent a severe limitation for some fundamental processes and QI applications where it is requested to operate with multipartite entanglement in a larger dimension Hilbert space [9]. This can be achieved by adopting nonlinear optical techniques, such

as the high gain parametric amplification, which allows us to entangle a large number of photons at the same time (multiparticle entanglement) [10] or by preparing two photons entangled in more than one degree of freedom and creating in this way a so-called hyperentangled state [11]. Other proposals aimed to increase the available Hilbert space concern the generation of d -level quantum systems (qudits) [12].

Hyperentangled states, spanning the 4×4 Hilbert space, permit us to operate with four qubits by using only two photons. It makes possible tasks which cannot be achieved with 2×2 entangled photon pairs, by using standard linear optics [13]. Among the others, the complete discrimination of the four orthogonal Bell states of Eq. (1) can be performed [11]. A further advantage of operating in a larger dimension Hilbert space deals with novel fundamental tests of quantum mechanics that exhibit a larger deviation from local realism and are more robust against noise [14].

The present work mainly concerns the controllable production, characterization, and utilization of two photon states, simultaneously entangled in polarization (π) and linear momentum (\mathbf{k}), which are generated by a single SPDC source of entanglement [15], with peculiar characteristics of flexibility in terms of state generation.

The work is organized as follows. In Sec. II, after a description of the source of hyperentanglement, we discuss the way to generate momentum entanglement and its characterization by quantum interferometry and Bell-Clauser-Horne-Shimony-Holt (CHSH) nonlocality tests. In Sec. III, a particular entanglement interferometry effect based on a delayed correlation technique. Section IV concerns the generation of hyperentanglement and the corresponding nonlocality tests performed in the degree of freedom of polarization and momentum. While Sec. V presents the results of an *all-versus-nothing* test of quantum nonlocality, recently obtained with hyperentangled states [16], the foreseeable perspectives of this method to generate hyperentangled states are outlined in Sec. VI.

II. MOMENTUM ENTANGLED STATES

The source adopted to generate photon pairs entangled in polarization and momentum is sketched in Fig. 1. As far as

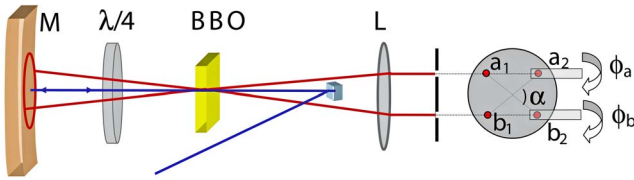


FIG. 1. (Color online) Layout of the source of polarization-momentum hyperentangled two-photon states. After the generation of a polarization entanglement, a lens L transforms the degenerate SPDC emission cone in a cylinder. Momentum entanglement is realized by a four hole screen which selects the correlated pairs of modes a_1, b_2 and a_2, b_1 . Momentum phase is adjusted by the fine rotation of two thin glass plates intercepting modes a_2 and b_1 .

polarization entanglement is concerned, a detailed description has been extensively given elsewhere [15]. In summary, the source consists of a high phase stability single arm interferometer in which the polarization entangled state $|\Phi\rangle = (1/\sqrt{2})(|H\rangle|H\rangle + e^{i\theta}|V\rangle|H\rangle)$ arises from the superposition of the degenerate parametric emission cones at wavelength λ of a 0.5 mm thick type-I β -BaB₂O₄ (BBO) crystal, excited in two opposite directions, by a V -polarized laser beam at wavelength $\lambda_p = \lambda/2$. Basic elements of the source, shown in the figure, are (i) a spherical mirror M , which reflects the pump beam and the parametric radiation at wavelength (wl) λ . (ii) A zero-order $\lambda/4$ waveplate (wp), placed within the M -BBO path, which performs the $|H\rangle|H\rangle \rightarrow |V\rangle|V\rangle$ transformation on the two-photon state belonging to the left emission cone (Fig. 1). (iii) A positive lens (L), which transforms the conical parametric emission of the crystal into a cylindrical one, whose transverse circular section identifies the so-called "entanglement-ring" ($e-r$). The insertion of a zero-order $\lambda/2$ wp in one of the output detection arms allows us to locally transform the state $|\Phi\rangle$ in the state $|\Psi\rangle = (1/\sqrt{2})(|H\rangle|V\rangle + e^{i\theta}|V\rangle|H\rangle)$ [HW*, Fig. 2(a)]. In this way, the overall radiation is expressed by the states $|\Psi^\pm\rangle$ and $|\Phi^\pm\rangle$ of Eq. (1), with phase θ ($0 \leq \theta \leq \pi$) easily controlled with high by micrometric displacements of the spherical mirror. Entangled states, either pure or controllable mixed states, have been created in a flexible way by this source [17,18]. Moreover, the nonlocal

character of the polarization entangled state generated by this source has been extensively demonstrated [19].

In a type-I crystal, the correlated \mathbf{k} directions belonging to the emission cone are intrinsically entangled. Hence, a two-photon momentum entangled state can be realized by selecting two pairs of symmetric modes, a_1 - b_2 and a_2 - b_1 , and analyzed by a beam splitter (BS) [20]. In our system, a four hole screen is aligned after the lens L in order to intercept the $e-r$ (cf. Fig. 1) [21]. The straight lines connecting, on the screen, the holes leaving through the correlated pairs intercross at an angle $\alpha = 18^\circ$. Because in SPDC process, the phase of the pump is transferred to any event allowed by phase and energy matching, the phase relation between the two pairs is $\phi = 0$, regardless the value of α . It can be easily set by suitable tilting of a thin glass plate (thickness $\delta \approx 200 \mu\text{m}$, refraction index $n = 1.52$) intercepting mode b_2 . When performing tests of Bell's inequality on momentum entanglement, a second glass plate is inserted on mode a_2 . In this case, the state phase is given by the sum of the two contributions $\phi = \phi_a + \phi_b$. For either one of the two SPDC cones, the momentum entangled Bell state

$$|\psi\rangle = \frac{1}{\sqrt{2}}(|a_1\rangle|b_2\rangle + e^{i\phi}|b_1\rangle|a_2\rangle) \quad (2)$$

is generated.

The radiation belonging to the modes a_1 - b_1 and a_2 - b_2 is divided along a vertical axis by a prismlike two-mirror system and then recombined onto a symmetric BS by the interferometric apparatus of Fig. 2(a). Figure 2(b) shows how modes a_1 and b_1 are spatially combined with modes a_2 and b_2 onto the BS. The four hole screen is mounted on a rotation stage in order to optimize the superposition. A trombone mirror assembly mounted on a motorized translation stage allows the fine adjustment of the path delay Δx between the two mode sets. Signals belonging to the output modes, a'_1, b'_1 and a'_2, b'_2 , are focused on four avalanche single-photon detectors ($D_{a'_1}, D_{b'_1}, D_{a'_2}, D_{b'_2}$ in Fig. 2(a)). This operation is achieved by the insertion of a mirror on each output arm, intercepting only modes b'_1 and b'_2 , M_1 and M_2 in Fig. 2. Four equal interfer-

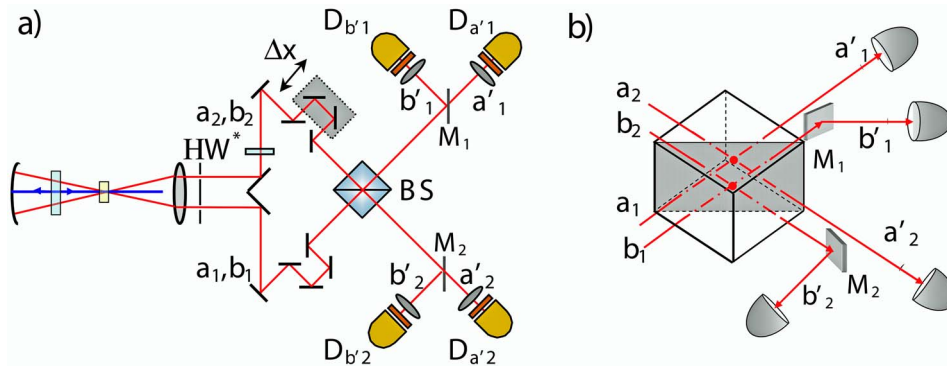


FIG. 2. (Color online) (a) Interferometric apparatus. Modes a_1 - b_1 and a_2 - b_2 , traveling along the two arms of the interferometer, are recombined onto a symmetric BS by translation Δx . The half wp (HW*) allows the transformation $|\Phi^\pm\rangle \rightarrow |\Psi^\pm\rangle$. Phase setting $\theta = 0$ or π is obtained by changing the distance of the spherical mirror with respect the BBO crystal. Pick-off mirrors M_1 and M_2 reflect modes b_1 and b_2 toward detectors $D_{b'_1}$ and $D_{b'_2}$. (b) Spatial coupling of the input modes a_1 - b_1 , a_2 - b_2 on the BS plane. The BS output modes, a'_1 - b'_1 , a'_2 - b'_2 are coupled to detectors $D_{a'_1}, D_{b'_1}, D_{a'_2}, D_{b'_2}$.

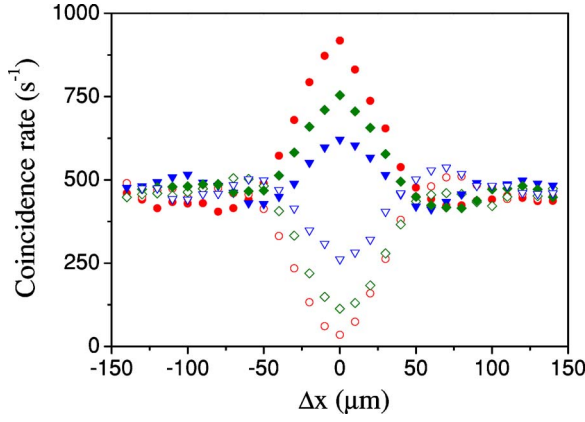


FIG. 3. (Color online) Interference pattern for the intermediate values of the momentum entanglement phase $0 \leq \phi \leq \pi$ obtained for several settings of the glass plate rotation angle. Time average of each experimental point: 10 sec.

ence filters, with bandwidth $\Delta\lambda=6$ nm, determine the coherence time of the emitted photons: $\tau_{coh} \approx 150$ fsec. Two-photon coincidences, $C(a'_i, b'_j)$ ($i, j=1, 2$), are registered for either one of the following mode combinations: $a'_1-b'_1$, $a'_1-b'_2$, $a'_2-b'_2$, $a'_2-b'_1$, while no coincidence is detected for $a'_1-a'_2$ and $b'_1-b'_2$. It is worth noting that, because of its particular configuration, which guarantees the mode matching of the two sets a_1-a_2 and b_1-b_2 over the same BS through a common path delay adjustment, the interferometric apparatus described above is insensitive to any fluctuation of the relative phase ϕ .

We characterized momentum entanglement by measuring the coincidences rate $C(a'_i, b'_j)$ as a function of Δx . The experimental results in Fig. 3, obtained by gradually varying the phase $\phi = \phi_a$ between 0 and π , demonstrate the triplet-singlet transition, $\phi=0 \rightarrow \phi=\pi$ of the momentum entangled state.

The expected coincidence count rate varies with ϕ as

$$C(a'_i, b'_j) \propto (1 \pm \cos \phi), \quad (3)$$

where the sign (+) holds for the combinations $D_{a'1}-D_{b'1}$ and $D_{a'2}-D_{b'2}$, and the sign (-) has to be taken for $D_{a'1}-D_{b'2}$ and $D_{a'2}-D_{b'1}$ [22]. The interference patterns shown in Fig. 4, obtained for $\Delta x=0$, by varying ϕ in the range $\pi/4 - (4/3)\pi$, with visibility, $V \approx 0.92$ for $D_{a'1}-D_{b'1}$ and $D_{a'2}-D_{b'2}$, and $V \approx 0.85$ for $D_{a'1}-D_{b'2}$ and $D_{a'2}-D_{b'1}$, confirm the behavior predicted by Eq. (3). The small phase shift observed between the crossed-path fringe patterns, $D_{a'1}-D_{b'2}$ and $D_{a'2}-D_{b'1}$, corresponds to an additional phase, $\Delta\phi=0.02\pi$, acquired by the reflected fields.

The entangled state $|\psi\rangle$ was also adopted to test the violation of a Bell inequality [23] by using the apparatus of Fig. 2(a) set at $\Delta x=0$. We measured the parameter S_k , which is expressed as

$$S_k = |E(\phi_a, \phi_b) - E(\phi_a, \phi_b^*) + E(\phi_a^*, \phi_b) + E(\phi_a^*, \phi_b^*)|, \quad (4)$$

where

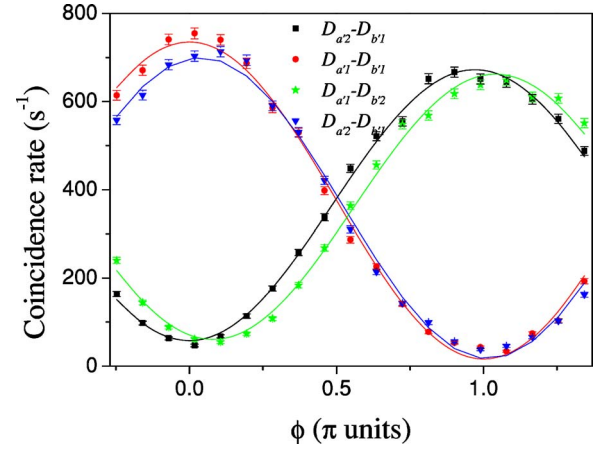


FIG. 4. (Color online) Interference fringes in the momentum rotated basis, measured by varying the phase ϕ for the detector combinations $D_{a'1}-D_{b'1}$, $D_{a'2}-D_{b'2}$, $D_{a'1}-D_{b'2}$, and $D_{a'2}-D_{b'1}$. Time average of each experimental point: 10 sec.

$$E(\phi_a, \phi_b) = \frac{C(a'_1, b'_1) + C(a'_2, b'_2) - C(a'_1, b'_2) - C(a'_2, b'_1)}{C(a'_1, b'_1) + C(a'_2, b'_2) + C(a'_1, b'_2) + C(a'_2, b'_1)}. \quad (5)$$

Two-photon coincidences were measured by using the phase setting $\phi_a=0$, $\phi_a^*=\pi/2$ and $\phi_b=\pi/4$, $\phi_b^*=(3/4)\pi$. The experimental value $S_k=2.6134 \pm 0.0036$, measured by integrating the data over 180 sec, corresponds to a violation as large as 170 standard deviations above the limit value $S_k=2$ implied by local realistic theories.

III. ENTANGLED NONLOCAL INTERFEROMETRY

Let us make some general comments on the results presented in Fig. 4, which demonstrate the effect of a continuous phase variation on the momentum entangled state. Some more considerations are necessary in order to enlighten the origin of the fringes. In the condition in which no glass plate is inserted on modes a_1 , a_2 , b_1 , b_2 , the coincidence count rate $C(a'_i, b'_j)$ corresponds to transmission and reflection of the correlated modes a_1-b_2 and a_2-b_1 , respectively. In these conditions, quantum indistinguishability arises from the mode matching of the respective probability amplitudes on the BS, $\Delta x=0$ [Fig. 5(a)]. Similar considerations are valid for the other cases, $C(a'_2, b'_1)$, $C(a'_1, b'_1)$, and $C(a'_2, b'_2)$.

When a glass plate with optical delay $\tau=n\delta/c > \tau_{coh}$ is inserted on mode b_2 , the original temporal matching cannot be restored since the delay τ between the photon wave packets belonging to modes a_1 and b_1 is not compensated by the apparatus [Fig. 5(b)]. At a first insight, any interference effect should be washed out in these conditions. Nevertheless, the results of Fig. 4 demonstrate that quantum interference is restored for a new value of $\Delta x = -c\tau/2$, which partially compensates the delay between modes a_2 and b_1 . In these conditions, the same path delay Δx has been added between modes a_1 and b_2 [Fig. 5(c)]. By the new setting, the probability amplitude of a photon emerging on mode b'_2 is delayed of the same amount with respect to that of a photon emerging on

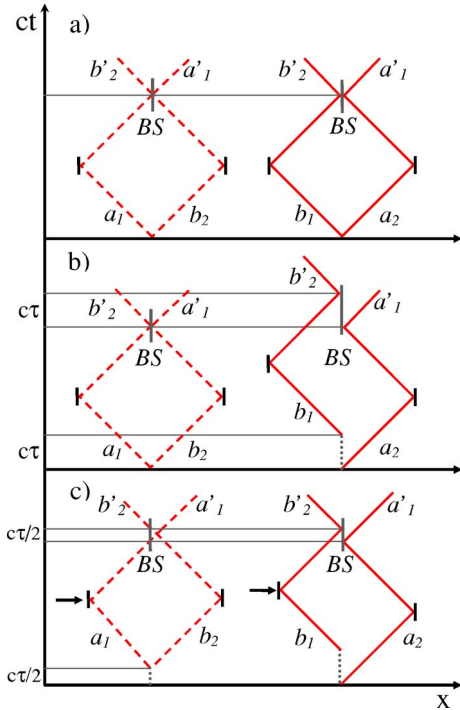


FIG. 5. (Color online) Feynman diagrams corresponding to the scattering of the incoming modes a_1, a_2, b_1, b_2 on the output modes a'_1 and b'_2 . (a) No external delay is inserted in the apparatus, $\tau=0$. Quantum interference arises from indistinguishability of the transmitted correlated modes a_1 - b_2 with the reflected ones a_2 - b_1 . (b) Absence of interference when the glass plate ($\tau > \tau_{coh}$) is inserted on mode b_2 . (c) Revival of quantum interference occurring for $\Delta x = -c\tau/2$.

mode a'_1 , regardless of the pair of holes which the photons have passed through. For instance, one is not allowed to distinguish whether the two photons were traveling over modes a_1 and b_2 , being reflected by BS, or emerging from modes a_2 and b_1 after transmission [Fig. 2(c)].

The same significant role of the entangled state in the superposition effect is found when the interference pattern of a polarization entangled state generated by a type-II NL crystal is investigated [22].

In general, the achievement of the interference condition *does not* imply the time superposition of the photon wave packets on the BS. Note, however, that in this case, quantum interference arises from the superposition of the probability amplitudes corresponding to two different photon pair generations with relative time delay $\tau/2$. Hence, the overall process consists of the overlapping of two analogous, but independent, interference processes having the same probability. It is worth noting that the two processes are indistinguishable if $\tau < \tau_p$, where τ_p corresponds to the coherence time of the pump laser. This condition is largely satisfied in the case of our experiment, where $\tau_p \geq 200$ psec.

The above arguments lead us to make some more considerations about the decoherence induced by the insertion of the glass plate on mode b_1 . The revival of quantum interference observed in the present experiment demonstrates the peculiar character of the induced decoherence. Similar to the photon echo effect observed for an atomic system with col-

lisionless inhomogeneous broadening, the disappearance of quantum interference is in our case fully reversible [24]. We could observe a similar effect in the case of generation of polarization entangled mixed states by the same source [17,18].

In order to more deeply analyze this phenomenon, we may consider the overall apparatus shown in Fig. 2(a) as the combination of two distinct, albeit interdependent, single-photon Mach-Zehnder interferometers (IFs). By referring to the optical setup of Fig. 2(a), they correspond respectively to the Alice (modes a_1 - a_2) and Bob sites (modes b_1 - b_2). Like in any standard IF, any phase change modifies the interference conditions but, differently from a standard IF, where the phase change is obtained by acting on the mutual optical delay between the two arms, in the present case, the phase coincides with that of the entangled state $|\psi\rangle$ and is common to both IFs. Because of these considerations, the apparatus of Fig. 2(a) may be interpreted as a modified version of the standard gated single-photon Mach-Zehnder IF [25]. In other words, the field belonging to the Bob IF is analyzed by assuming as “gates,” the two signals at the output of the Alice IF or vice versa. This reproduces exactly the interference fringe behavior indicated by Eq. (3). It is demonstrated by the experimental results of Fig. 4, carried out nonlocally by the two sets of detectors, $D_{a'_1}D_{b'_1}$ and $D_{a'_2}D_{b'_2}$. These results can be obtained only if the state $|\psi\rangle$ is entangled, as said.

IV. POLARIZATION-MOMENTUM HYPERENTANGLED STATES

The hyperentangled state realized in the present experiment by simultaneously entangling two photons in polarization and momentum, is expressed as

$$\begin{aligned}
 |\Xi\rangle &= |\Psi\rangle \otimes |\psi\rangle \\
 &= \frac{1}{2}(|H\rangle|V\rangle + e^{i\theta}|V\rangle|H\rangle) \otimes (|a_1\rangle|b_2\rangle + e^{i\phi}|b_1\rangle|a_2\rangle).
 \end{aligned} \tag{6}$$

The relevant cases $|\Xi^{\pm\pm}\rangle = |\Psi^{\pm}\rangle \otimes |\psi^{\pm}\rangle$ correspond to the phase values $\theta=0, \pi$ for $|\Psi^{\pm}\rangle$ and $\phi=0, \pi$ for $|\psi^{\pm}\rangle$. We can express $|\Xi\rangle$ in terms of the creation operators of the electromagnetic field applied to the vacuum state

$$|\Xi\rangle = \frac{1}{2} \{ a_{1H}^\dagger b_{2V}^\dagger + e^{i\theta} a_{1V}^\dagger b_{2H}^\dagger + e^{i\phi} b_{1H}^\dagger a_{2V}^\dagger + e^{i(\theta+\phi)} b_{1V}^\dagger a_{2H}^\dagger \} |0\rangle \tag{7}$$

with $a_{j\sigma}^\dagger$ and $b_{j\sigma}^\dagger$ representing the operators associated to modes a_j, b_j ($j=1,2$) with polarization σ ($\sigma=H, V$).

By applying the BS input-output relations [26], it is easy to express $|\Xi\rangle$ as a function of the operators associated to the BS output modes a'_j, b'_j

$$|\Xi\rangle = \frac{1}{4} \left\{ \begin{aligned} & \left[a_{1H}^\dagger b_{2V}^\dagger (1 - e^{i(\theta+\phi)}) + a_{2H}^\dagger b_{2V}^\dagger (1 + e^{i(\theta+\phi)}) \right. \\ & \left. - a_{1H}^\dagger b_{1V}^\dagger (1 + e^{i(\theta+\phi)}) - a_{2H}^\dagger b_{1V}^\dagger (1 - e^{i(\theta+\phi)}) \right] \\ & + e^{i\theta} \left[a_{1V}^\dagger b_{2H}^\dagger (1 - e^{i(\phi-\theta)}) + a_{2V}^\dagger b_{2H}^\dagger (1 + e^{i(\phi-\theta)}) - \right. \\ & \left. a_{1V}^\dagger b_{1H}^\dagger (1 + e^{i(\phi-\theta)}) - a_{2V}^\dagger b_{1H}^\dagger (1 - e^{i(\phi-\theta)}) \right] \end{aligned} \right\} |0\rangle \quad (8)$$

The expected number of coincidences at the BS output ports is given by the following expression:

$$C(a'_{i\sigma}, b'_{i\rho}) \propto [1 + \cos(\phi \pm \theta)], \quad (9)$$

$$C(a'_{i\sigma}, b'_{j\rho}) \propto [1 - \cos(\phi \pm \theta)] \quad (10)$$

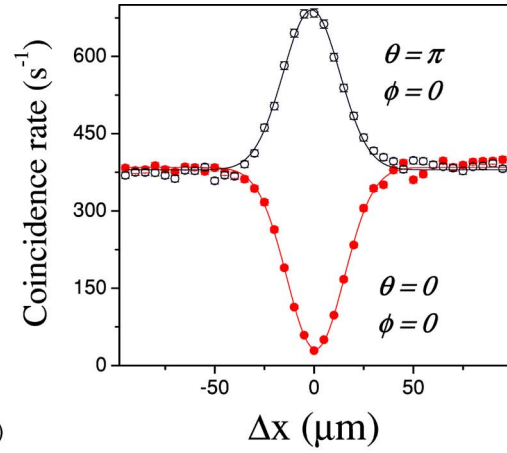
($i, j=1, 2$) where (+) sign has to be taken for $\sigma=H$ and $\rho=V$ and (−) sign holds for $\sigma=V$ and $\rho=H$. It comes out that $C(a'_i, b'_j)$ vanishes in the cases $|\Xi^{++}\rangle, |\Xi^{--}\rangle$, while it is maximized for $|\Xi^{+-}\rangle, |\Xi^{-+}\rangle$ at $\Delta x=0$. This behavior can be understood in terms of the symmetric or antisymmetric character of the states $|\Xi^{\pm\pm}\rangle$. Nevertheless, this phenomenon does not originate from bosonic coalescence of the photons, as in standard Ou-Mandel effect [26]. Note that, for the hyperentangled states $|\Pi\rangle = |\Phi^\pm\rangle \otimes |\psi^\pm\rangle$, no peak-dip transition is expected for θ varying from 0 to π , since the states $|\Phi^\pm\rangle$ are symmetric, regardless the value of the phase θ .

Manipulation of the state $|\Xi\rangle$ was performed by varying independently θ and ϕ . In particular, the experimental results of Figs. 6(a) and 6(b) show the characteristic quantum interference patterns obtained by measuring $C(a'_1, b'_1)$ as a function of Δx . The transition from the symmetric ($|\Xi^{++}\rangle$) to the antisymmetric ($|\Xi^{+-}\rangle$) state condition upon change of the phase θ is shown with a resonance “visibility” ≈ 0.90 [Fig. 6(a)]. In the same way, by setting $\theta=0$, we observe a peak for $\phi=0$ or a dip for $\phi=\pi$ [Fig. 6(b)]. Similar results were obtained for the other photon pair coincidences $C(a'_1, b'_2)$, $C(a'_2, b'_1)$, $C(a'_2, b'_2)$, measured, by varying either θ or ϕ .

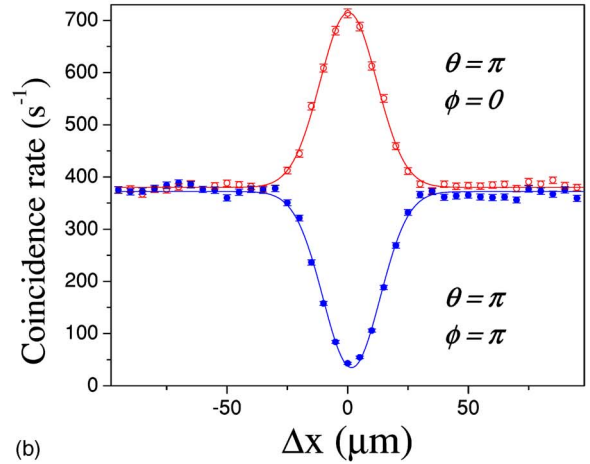
By measuring the coincidence rate $C(a'_1, b'_1)$ in the path delay condition $\Delta x=0$, we could measure the interference fringes on the diagonal basis of the polarization shown in Fig. 7(a). In this case, a $\lambda/2$ wp was kept fixed at $\pi/8$ on mode a_1 , while the polarization on mode b_1 was tuned by an other $\lambda/2$ wp. Finally, the experimental results given in Fig. 7(b) correspond to the interference behavior of $C(a'_1, b'_1)$ obtained as a function of the momentum phase ϕ for $\theta=0$. The high value of interference visibility reported demonstrates the quality of entanglement in the two degrees of freedom.

V. NONLOCALITY TEST WITH HYPERENTANGLED STATES

The nonlocal character of the hyperentangled state $|\Xi\rangle$ was first verified by performing two separate Bell-CHSH tests on momentum and polarization. By averaging over 180 sec, we could measure in the first case $S_k = 2.3332 \pm 0.0033$, which corresponds to a violation of local realism by 102 standard deviations. In the second experiment, concerning polarization correlation, we obtained $S_\pi = 2.4525 \pm 0.0034$ by lasting the same average time. The cor-



(a)



(b)

FIG. 6. (Color online) Coincidence rate $C(a'_1, b'_1)$ vs Δx for the state $|\Xi\rangle$. (a) $\theta=0, \phi=0$ (symmetric state), ($V=0.92$), $\theta=\pi, \phi=0$ (antisymmetric state), ($V=0.82$). (b) $\theta=\pi, \phi=\pi$ (symmetric state), ($V=0.90$); $\theta=\pi, \phi=0$ (antisymmetric state), ($V=0.88$). The corresponding experimental fits are also shown. The full width at half maximum ($\approx 30 \mu\text{m}$) of the interference patterns is in agreement with the expected value for a filter bandwidth $\Delta\lambda=6 \text{ nm}$. Time average of each experimental point: 10 sec.

responding violation is equal to 130 standard deviations with respect to the limit value $S_\pi=2$ implied by local realistic theories.

The above results only indirectly demonstrate the nonlocal character of the state $|\Xi\rangle$, since the measurements involve only one degree of freedom each time. We can exploit the hyperentangled state as a whole (4×4) system for a nonlocality test which represents a generalization of the Greenberger-Horne-Zeilinger (GHZ) argument to the case of two observers [9,27]. This purely logical proof is based on the impossibility to attribute a fixed value to single particle observables, without incurring inconsistent predictions. Nevertheless, an inequality is necessary as a quantitative test, since the exact correlations needed for the proof are never observed in a real experiment because of unavoidable imperfections. The test exploits the fact that the hyperentangled state $|\Xi^{--}\rangle = |\Psi^-\rangle \otimes |\psi^-\rangle$ is an eigenstate of the operators

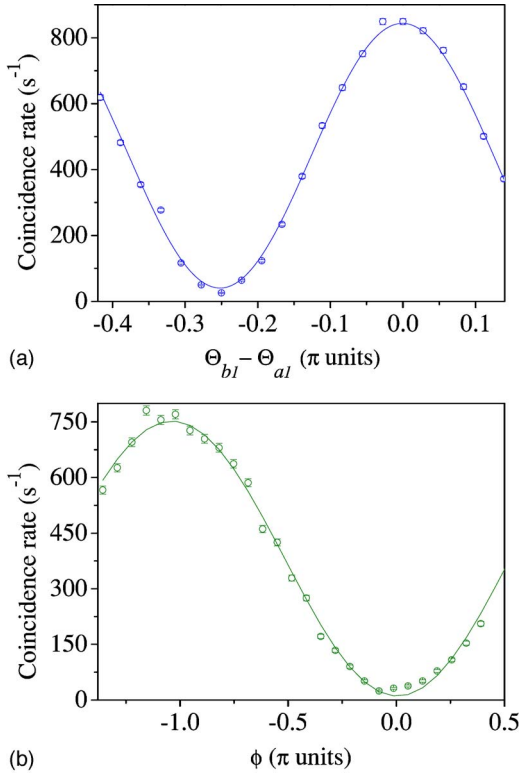


FIG. 7. (Color online) Interference pattern on the coincidence rate $C(a'_1, b'_1)$ obtained (a) on the diagonal basis of the polarization ($V=0.91$). θ_{a1} and θ_{b1} represent the angular settings of the two $\lambda/2$ wp's on modes a_1 and b_1 , (b) as a function of ϕ . Polarization entanglement phase $\theta=0$ ($V=0.97$). Time average of each experimental point: 10 sec.

$$\begin{aligned}
 z_1 z_2 |\Xi^{--}\rangle &= -|\Xi^{--}\rangle, & z'_1 z'_2 |\Xi^{--}\rangle &= -|\Xi^{--}\rangle, \\
 x_1 x_2 |\Xi^{--}\rangle &= -|\Xi^{--}\rangle, & x'_1 x'_2 |\Xi^{--}\rangle &= -|\Xi^{--}\rangle, \\
 z_1 z'_1 z_2 z'_2 |\Xi^{--}\rangle &= |\Xi^{--}\rangle, & x_1 x'_1 x_2 x'_2 |\Xi^{--}\rangle &= |\Xi^{--}\rangle, \\
 z_1 x'_1 z_2 x'_2 |\Xi^{--}\rangle &= |\Xi^{--}\rangle, & x_1 z'_1 x_2 z'_2 |\Xi^{--}\rangle &= |\Xi^{--}\rangle, \\
 z_1 z'_1 x_1 x'_1 \cdot z_2 x'_2 x_2 z'_2 |\Xi^{--}\rangle &= -|\Xi^{--}\rangle. & & (11)
 \end{aligned}$$

In the above expression, the following Pauli operators have been introduced:

$$z_i = \sigma_{z_i} = |H\rangle\langle H| - |V\rangle\langle V|, \quad x_i = \sigma_{x_i} = |H\rangle\langle V| + |V\rangle\langle H|$$

$$(i = 1, 2),$$

$$z'_1 = \sigma'_{z_1} = |a_1\rangle\langle a_1| - |a_2\rangle\langle a_2|, \quad x'_1 = \sigma'_{x_1} = |a_1\rangle\langle a_2| + |a_2\rangle\langle a_1|,$$

$$(12)$$

$$z'_2 = \sigma'_{z_2} = |b_1\rangle\langle b_1| - |b_2\rangle\langle b_2|, \quad x'_2 = \sigma'_{x_2} = |b_1\rangle\langle b_2| + |b_2\rangle\langle b_1|.$$

$$(13)$$

By properly combining the above predictions, we can estimate the expectation value of the operator

$$\begin{aligned}
 O = & -z_1 z_2 - z'_1 z'_2 - x_1 x_2 - x'_1 x'_2 + z_1 z'_1 z_2 z'_2 + x_1 x'_1 x_2 x'_2 \\
 & + z_1 x'_1 z_2 x'_2 + x_1 z'_1 x_2 z'_2 - z_1 z'_1 x_1 x'_1 \cdot z_2 x'_2 x_2 z'_2.
 \end{aligned}$$

$$(14)$$

It is found $\langle O \rangle = 9$ [9] and a proper limit imposed by local realism for $\langle O \rangle$ needs to be found. Indeed, the examined system is not equivalent to a four particle state located in four spatially separated sites, since polarization and momentum are carried by the same photon. Thus, the hidden variable model has to describe the presence of local $(\pi-\mathbf{k})$ correlations. This represents a relevant difference from the standard four particle GHZ proof, where one is allowed to consider each particle as completely separated from the other three ones. On the contrary, the present nonlocality test involves two observers dealing with a four level system. On the basis of these remarks, the following limit is found: $\langle O \rangle \leq 7$.

The evaluation of $\langle O \rangle$ is given by the measurement of the nine operators appearing in Eq. (14). The violation can be observed if the minimum value of entanglement visibility is $7/9$ [9]. The measured visibilities of polarization and momentum entanglement obtained by our system (Figs. 6 and 7) are suitable on this purpose. The experimental apparatuses implemented to observe violation are sketched in Figs. 8(a) and 8(b). In the present experiment, Alice and Bob perform the measurements by the upper ($D_{a'1} - D_{a'2}$) and lower ($D_{b'1} - D_{b'2}$) detectors, respectively. By referring to the optical setup of Fig. 8(a), the modes $a_1 - a_2$ and $b_1 - b_2$ are sent directly to the Alice and Bob sites for the measurement of the operators $z_1 z_2$, $z'_1 z'_2$, and $z_1 z'_1 z_2 z'_2$. In this way, the momentum is analyzed in the natural basis and, at the same time, the signal polarization is analyzed in the $H-V$ by a $\lambda/2$ wp (HW) and a polarizing beam splitter (PBS) before each detector. We could evaluate the expectation values $z_1 z_2$, $z'_1 z'_2$, and $z_1 z'_1 z_2 z'_2$ as follows:

$$\begin{aligned}
 \langle z_1 z_2 \rangle = & \frac{1}{N} \sum_{i,j=1,2} C(a_{iH}, b_{jH}) + C(a_{iV}, b_{jV}) - C(a_{iH}, b_{jV}) \\
 & - C(a_{iV}, b_{jH}),
 \end{aligned}$$

$$(15)$$

$$\begin{aligned}
 \langle z'_1 z'_2 \rangle = & \frac{1}{N} \sum_{\sigma, \rho=H,V} C(a_{1\sigma}, b_{1\rho}) + C(a_{2\sigma}, b_{2\rho}) - C(a_{1\sigma}, b_{2\rho}) \\
 & - C(a_{2\sigma}, b_{1\rho}),
 \end{aligned}$$

$$(16)$$

$$\begin{aligned}
 \langle z_1 z'_1 z_2 z'_2 \rangle = & \frac{1}{N} \sum_{i,j=1,2} (-1)^{i+j} [C(a_{iH}, b_{jH}) + C(a_{iV}, b_{jV}) \\
 & - C(a_{iH}, b_{jV}) - C(a_{iV}, b_{jH})],
 \end{aligned}$$

$$(17)$$

$$N = \sum_{i,j=1,2} \sum_{\sigma, \rho=H,V} C(a_{i\sigma}, b_{j\rho}).$$

$$(18)$$

The operators $x_1 x_2$ and $x_1 z'_1 x_2 z'_2$ could be evaluated by the same apparatus, by analyzing the polarization in the $D-D^*$ basis, with $D = 2^{-1/2}(H+V)$ and $D^* = 2^{-1/2}(H-V)$ and using similar formulas to the ones given in Eq. (15)

Figure 8(b) shows the optical setup used for the measurement of $x'_1 x'_2$, $x_1 x'_1 x_2 x'_2$, and $z_1 z'_1 z_2 z'_2$. Before being analyzed

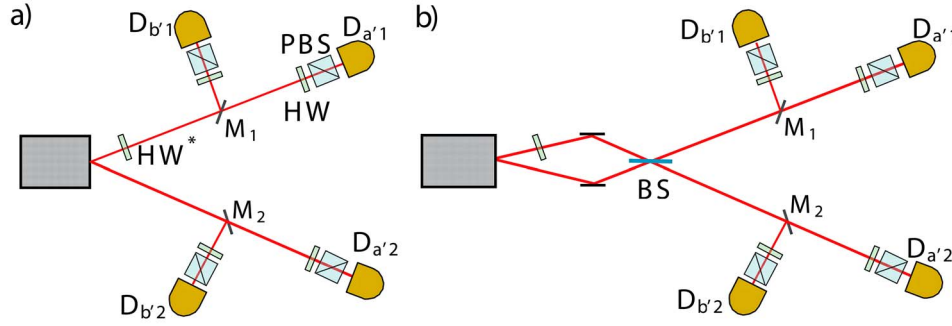


FIG. 8. (Color online) Experimental apparatus to measure the expectation values of the nine operators compared in O . (a) Modes a_1 , b_1 , a_2 , and b_2 are directly coupled to detectors; polarization analysis is performed in the orthonormal bases, either H - V or D - D^* , by rotating the half wave plates HW before the detectors. The half wave plate HW* performing the $|\Phi\rangle \rightarrow |\Psi\rangle$ transformation is also shown. M_1 and M_2 are the pick-off mirrors. By this configuration, one can evaluate the values of $z_1 z_2$, $x_1 x_2$, $z_1' z_2'$, $z_1 z_1' z_2 z_2'$, and $x_1 x_1' x_2 x_2'$. (b) The two mode sets a_1 - b_1 and a_2 - b_2 are spatially combined onto the BS before being coupled to detectors. In this way, one can perform the transformation on the momentum basis and measure the values of $x_1' x_2'$, $x_1 x_1' x_2 x_2'$, and $z_1 x_1' z_2 x_2'$. The same apparatus is used for performing the Bell state analysis by removing the HW* plate in order to evaluate the value of $z_1 z_1' x_1 x_1' \cdot z_2 x_2' x_2 z_2'$.

in each arm and coupled to detectors, the two mode sets a_1 - b_1 and a_2 - b_2 are spatially combined onto the BS, which performs the transformation from the natural basis a_1 - a_2 to the rotated basis d - d^* , where $d = 2^{-1/2}(a_1 + a_2)$ and $d^* = 2^{-1/2}(a_1 - a_2)$. The same transformation was performed on modes b_1 and b_2 .

Concerning the last term, $z_1 z_1' x_1 x_1' \cdot z_2 x_2' x_2 z_2'$, we note that the eigenstates of the single photon operator $z_1 z_1' x_1 x_1'$ correspond to the Bell states

$$\frac{1}{\sqrt{2}}(|H\rangle|a_1\rangle \pm |V\rangle|a_2\rangle), \quad (19)$$

$$\frac{1}{\sqrt{2}}(|V\rangle|a_1\rangle \pm |H\rangle|a_2\rangle). \quad (20)$$

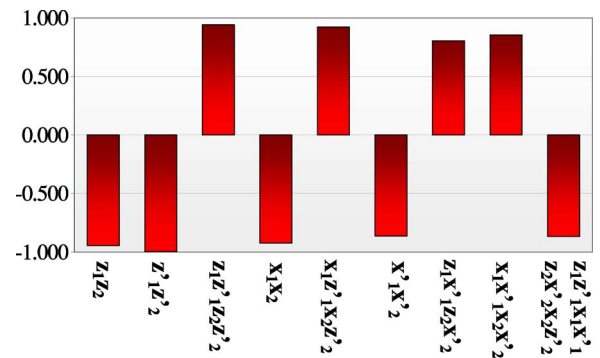
Hence, the evaluation of $z_1 z_1' x_1 x_1' \cdot z_2 x_2' x_2 z_2'$ is equivalent to realize the Bell state analysis already performed in the teleportation experiment of Ref. [5] on both particles. For this purpose, we need to rotate the polarization on both modes a_1 and b_1 before recombining them onto the BS, by simply removing the $\lambda/2$ wp which performs the $|\Phi^-\rangle \rightarrow |\Psi^-\rangle$ transformation (HW* in Fig. 8). In this measurement, Alice's and Bob's detectors, $(D_{a'1}$ - $D_{a'2})$ and $(D_{b'1}$ - $D_{b'2})$ perform the measurements in the H - V basis.

The whole experiment has been carried out by a sequence of measurements each one lasting an average time of 30 sec. The results corresponding to the measurement of the nine terms of O are summarized in the histogram shown in Fig. 9. The experimental value of $\langle O \rangle$, obtained after summation of the whole set of the measured values is $\langle O \rangle = 8.114 \pm 0.011$. It corresponds to a violation of the inequality by 101 standard deviations, demonstrating in this way a large contradiction with local realism. The experiment described above gives a strong evidence of the nonlocal character of the hyperentangled state. However, it requires supplementary assumptions with respect to those assumed in the original proposal, where one should deal with the values of z_1 , z_1' , and $z_1 z_1'$, namely $v(z_1)$, $v(z_1')$, and $v(z_1 z_1')$, as three unrelated elements

of reality [9]. In our experiment the same apparatus of Fig. 8(a) is used for measuring either the product $v(z_1)v(z_1')$ or the value $v(z_1 z_1')$, implicitly assuming that $v(z_1 z_1') = v(z_1)v(z_1')$. The same argument holds for the measurement of the operators: x_1 , x_1' , and $x_1 x_1'$, z_2 , x_2' , and $z_2 x_2'$, x_2 , z_2' , and $x_2 z_2'$ [28].

VI. CONCLUSION

In this paper, we have presented a parametric source of $(\pi$ - \mathbf{k}) hyperentangled photon states given by Eq. (6). These states are given by the typical momentum-spin correlation arising in any SPDC process. By this device, besides polarization entanglement, realized by means of a high stability interferometric scheme [15], it is possible to adopt the intrinsic, stable entanglement of the whole set of \mathbf{k} modes belonging to the emission cone of a type-I NL crystal [11]. The



$$7 \leq \langle \hat{O} \rangle = 8.114 \pm 0.011 \leq 9$$

FIG. 9. (Color online) Bar chart of expectation values for the nine operators involved in the experiment. The following results have been obtained: $z_1 z_2 = -0.9428 \pm 0.0030$, $z_1' z_2' = -0.9953 \pm 0.0033$, $z_1 z_1' z_2 z_2' = 0.9424 \pm 0.0030$, $x_1 x_2 = -0.9215 \pm 0.0033$, $x_1 x_1' x_2 x_2' = 0.9217 \pm 0.0033$, $x_1' x_2' = -0.8642 \pm 0.0043$, $z_1 x_1' z_2 x_2' = 0.8039 \pm 0.0040$, $x_1 x_1' x_2 x_2' = 0.8542 \pm 0.0040$, $z_1 z_1' x_1 x_1' \cdot z_2 x_2' x_2 z_2' = -0.8678 \pm 0.0043$.

entanglement behavior and the nonlocal character of the $(\pi\text{-}\mathbf{k})$ two-photon state have been deeply investigated. In particular, an all-versus-nothing test of nonlocality conceived for two observers was performed [16].

The high entanglement visibilities obtained by this device may open interesting perspectives for possible applications of hyperentangled states in quantum information. Indeed, these states allow to discriminate among the entire set of Bell states, either encoded in polarization or momentum qubits. In particular, hyperentangled states can be employed in an experimental scheme in which a PBS acts as a controlled-NOT gate. There polarization acts as the control qubit and momentum as the target qubit [20]. The same optical scheme could also be employed to realize an entanglement purification technique, in which polarization entanglement is concentrated by exploiting the correlation within momentum state [29]. Another perspective is given by the adoption of the \mathbf{k} momentum entanglement existing in the conical emission of the NL crystal to realize high dimensional entangled systems

by using the spatial degree of freedom. Besides polarization and linear momentum, photon pairs simultaneously entangled in three degrees of freedom may be produced by this source. This could be done by including energy-time entanglement, which is implicitly present in any SPDC process [30]. More in general, the high phase $\theta\text{-}\phi$ stability of the $(\pi\text{-}\mathbf{k})$ entanglement achieved by this source allows to conceive new schemes of joint entanglement over the two vector degrees of freedom for the realization of quantum cryptographic schemes [12,31]. For this purpose, an upgraded version of this system implies the coupling of the four modes a_1, b_2, a_2, b_1 to single mode optical fibers.

ACKNOWLEDGMENTS

This work was supported by the FET European Network on Quantum Information and Communication (Contract No. IST-2000-29681: ATESIT), FIRB-MIUR 2001, and PRA-INFN 2002 (CLON).

-
- [1] A. Ekert and R. Jozsa, *Rev. Mod. Phys.* **68**, 733 (1996); E. Knill, R. Laflamme, and G. J. Milburn, *Nature (London)* **409**, 46 (2001).
- [2] C. H. Bennett, G. Brassard, C. Crepeau, R. Jozsa, A. Peres, and W. K. Wootters, *Phys. Rev. Lett.* **70**, 1895 (1993).
- [3] A. Ekert, *Nature (London)* **358**, 14 (1992); N. Gisin, G. Ribordy, W. Tittel, and H. Zbinden, *Rev. Mod. Phys.* **74**, 145 (2002).
- [4] C. H. Bennett and S. J. Wiesner, *Phys. Rev. Lett.* **69**, 2881 (1992); K. Mattle, H. Weinfurter, P. G. Kwiat, and A. Zeilinger, *ibid.* **76**, 4656 (1996).
- [5] D. Boschi, S. Branca, F. De Martini, L. Hardy, and S. Popescu, *Phys. Rev. Lett.* **80**, 1121 (1998).
- [6] D. Bouwmeester, J. M. Pan, K. Mattle, M. Eibl, H. Weinfurter, and A. Zeilinger, *Nature (London)* **390**, 575 (1997); I. Marcikic *et al.*, *ibid.* **421**, 509 (2003).
- [7] J. W. Pan, D. Bouwmeester, H. Weinfurter, and A. Zeilinger, *Phys. Rev. Lett.* **80**, 3891 (1998); T. Jennewein, G. Weihs, J. W. Pan, and A. Zeilinger, *ibid.* **88**, 017903 (2002); F. Sciarrino, E. Lombardi, G. Milani, and F. De Martini, *Phys. Rev. A* **66**, 024309 (2002).
- [8] D. Klyshko, *Photons and Nonlinear Optics* (Gordon and Breach, New York, 1988).
- [9] A. Cabello, *Phys. Rev. Lett.* **87**, 010403 (2001); Z. B. Chen, J. W. Pan, Y. D. Zhang, C. Brukner, and A. Zeilinger, *ibid.* **90**, 160408 (2003).
- [10] F. De Martini, F. Sciarrino, and V. Secondi, e-print quant-ph/0410225, *Phys. Rev. Lett.* (to be published).
- [11] P. G. Kwiat, *J. Mod. Opt.* **44**, 2173 (1997); P. G. Kwiat and H. Weinfurter, *Phys. Rev. A* **58**, R2623 (1998).
- [12] H. Bechmann-Pasquinucci and A. Peres, *Phys. Rev. Lett.* **85**, 3313 (2000); R. T. Thew, A. Acin, H. Zbinden, and N. Gisin, *Quantum Inf. Comput.* **4**, 93 (2004); G. M. D'Ariano, P. Mataloni, and M. F. Sacchi, *Phys. Rev. A* **71**, 062337 (2005).
- [13] S. Ghosh, G. Kar, A. Roy, A. Sen (De), and U. Sen, *Phys. Rev. Lett.* **87**, 277902 (2001); J. Calsamiglia and N. Lukenhaus, *Appl. Phys. B: Lasers Opt.* **72**, 67 (1999).
- [14] D. Collins, N. Gisin, N. Linden, S. Massar, and S. Popescu, *Phys. Rev. Lett.* **88**, 040404 (2002); D. Kaszlikowski, L. C. Kwek, J.-L. Chen, M. Zukowski, and C. H. Oh, *Phys. Rev. A* **65**, 032118 (2002).
- [15] C. Cinelli, G. Di Nepi, F. De Martini, M. Barbieri, and P. Mataloni, *Phys. Rev. A* **70**, 022321 (2004).
- [16] C. Cinelli, M. Barbieri, F. De Martini, and P. Mataloni, e-print quant-ph/0505098, *Phys. Rev. Lett.* (to be published).
- [17] M. Barbieri, F. De Martini, G. Di Nepi, P. Mataloni, G. M. D'Ariano, and C. Macchiavello, *Phys. Rev. Lett.* **91**, 227901 (2003).
- [18] M. Barbieri, F. De Martini, G. Di Nepi, and P. Mataloni, *Phys. Rev. Lett.* **92**, 177901 (2004).
- [19] M. Barbieri, F. De Martini, G. Di Nepi, and P. Mataloni, *Phys. Lett. A* **334**, 23 (2005).
- [20] S. P. Walborn, S. Padua, and C. H. Monken, *Phys. Rev. A* **68**, 042313 (2003).
- [21] C. Cinelli, M. Barbieri, F. De Martini, and P. Mataloni, *Laser Phys.* **15**, 1 (2005).
- [22] G. Di Giuseppe, F. De Martini, D. Boschi, and S. Branca, *Fortschr. Phys.* **46**, 643 (1998).
- [23] J. G. Rarity and P. R. Tapster, *Phys. Rev. Lett.* **64**, 2495 (1990).
- [24] N. A. Kurnit, I. D. Abella, and S. R. Hartmann, *Phys. Rev. Lett.* **13**, 567 (1964).
- [25] P. Grangier, G. Roger, and A. Aspect, *Europhys. Lett.* **1**, 173 (1986).
- [26] R. Loudon, *The Quantum Theory of Light* (Clarendon Press, Oxford, 2000), Chaps. 5 and 6.
- [27] T. Yang *et al.*, e-print quant-ph/0502085, *Phys. Rev. Lett.* (to be published).
- [28] A. Cabello, private communication.
- [29] C. Simon and J.-W. Pan, *Phys. Rev. Lett.* **89**, 257901 (2002).
- [30] J. T. Barreiro *et al.*, e-print quant-ph/0507128.
- [31] Z. Zhao *et al.*, e-print quant-ph/0211098.